Proceedings of ASME Turbo Expo 2011
GT2011
June 6-10, 2011, Vancouver, British Columbia, Canada

GT2011-45585

EXPERIMENTAL INVESTIGATION OF LOUVER COOLING SCHEME ON GAS TURBINE VANE SUCTION SIDE

Elnady T.[*], Hassan O.[*], Hassan I.[*], Kadem L.[*], and Lucas T.[**]

[*]Department of Mechanical and Industrial Engineering, Concordia University, Montreal, QC, H3G1M8, Canada
[**] Chief, Turbine Cooling and Static Structures, Pratt and Whitney Canada, Longueuil, QC, J4G 1A1, Canada

ABSTRACT:

An experimental investigation has been performed to measure the film cooling performance of louver scheme over a scaled vane of high-pressure gas turbine using a two-dimensional cascade. Two rows of axially oriented louver scheme are used to cool the suction side and their performance is compared with two similar rows of standard cylindrical holes. The effect of hole location on the cooling performance is investigated for each row individually, then the row interaction is investigated for both rows at four different blowing ratios ranging from 1 to 2 with a 0.9 density ratio. The exit Reynolds number based on the true chord is 1.5E5 and exit Mach number is 0.23. The temperature distribution on the vane is mapped using a transient Thermochromic Liquid Crystal (TLC) technique to obtain the local distributions of the heat transfer coefficient and film cooling effectiveness. The louver scheme shows a superior cooling effectiveness than that of the cylindrical holes at all blowing ratios in terms of protection and lateral coverage. The row location highly affects the cooling performance for both the louver and cylindrical scheme.

NOMENCLATURE

C	true chord (cm)
C_p	specific heat capacity (J/kg.K)
C_x	axial chord (cm)
d	hole diameter (mm)
H	hue value
h	heat transfer coefficient with film cooling ($W/m^2.K$)
h_o	heat transfer coefficient without film cooling
k	thermal conductivity (W/m.K)
L	actual chord (cm)
l	hole length (mm)
p	pitch (distance between two holes) (mm)
q	heat load (W)
s	vane surface distance (cm)
T	temperature (K)
T_i	Initial temperature of the surface (K)
t	time (sec)
v	velocity (m/s)
x	distance downstream the hole exit (mm)
z	spanwise distance between holes (mm)

Greeks

α	thermal diffusivity (m^2/s)
β	compound angle (degree)
γ	specific heats ratio
η	film cooling effectiveness
λ	Inclination angle (degree)
ρ	density (kg/m^3)

Subscripts

c	coolant
elec	electric
f	film
j	jet
loss	losses
m	main flow
o	total
w	wall (surface)

Acronyms

B.R.	Blowing Ratio $[(\rho v)_j/(\rho v)_m]$
D.R.	Density Ratio (ρ_j/ρ_m)
P.R.	Pressure Ratio (P_j/P_m)
PSP	Pressure Sensitive Paint
RGB	Red, Green, and Blue
ROI	Region Of Interest
TLC	Thermochromic Liquid Crystal

INTRODUCTION

With an elevated importance on environmental sustainability and the depletion in fossil fuel resources around the world, it has become increasingly necessary to improve the efficiency and hence increase the power/weight ratio for the next generation of gas turbines. Increasing the temperature of combustion products demands a development in the cooling capacity of the gas turbine components. Many studies have shown that standard cylindrical holes permit some cooling to the hot surfaces, however, contouring the exit geometry provides an elevated protection with better lateral coverage.

Goldstein et al. [1] experimentally investigated the effect of the hole exit shaping compared with the cylindrical exit. They reported a significant increase in the cooling effectiveness of the shaped exit with the better lateral coverage. They attributed this increase to the reduction of the jet exit velocity, causing a momentum reduction and allowing the jet to remain attached to the surface. Gritsch et al. [2] compared experimentally the performance of three different cooling holes. The hole geometries included a laid-back fan shaped hole, a fan shaped hole, and the standard cylindrical hole. Their findings emphasized the improved performance of the shaped holes particularly the former geometry. The double modification on the hole geometry decreased the jet momentum and increased the lateral coverage. With the same hole shaping, Yu et al. [3] studied the heat transfer distribution in addition to the cooling effectiveness using a transient TLC technique, and they supported their findings with laser-sheet flow visualization. The lateral-forward shaped provided better heat transfer enhancement compared with the cylindrical exit with close, but not better, enhancement to the lateral shape. In two companion studies, Yuen et al. [4] experimentally investigated the interaction between two rows with different arrangements. They reported better cooling effectiveness and heat transfer enhancement in the double rows injection compared with one row even for the same injected mass flow. The in-line arrangement is better than the staggered one in terms of lateral-average performance; however, the stagger arrangement provided better lateral coverage with more uniformity over the surface.

All of the pre-mentioned studies were conducted on a flat plate with axial-oriented holes. The flow physics on the highly curved surfaces, such as an actual turbine airfoil, differ from the flow physics on a flat surface. Therefore, several research studies have been conducted to investigate and quantify the film cooling performance over actual turbine airfoils. Teng et al. [5] reported better heat transfer enhancement of two shaped holes, laidback fan-shaped and fan-shaped, compared with the cylindrical exit on the gill region of a gas turbine blade. Concluding with the same results, Dittmar et al. [6] performed their measurements on a model of vane suction side. Zhang and Moon [7] using PSP, investigated the effect of shaped hole location on thecooling effectiveness over a blade suction side in a linear cascade. They noticed an increase in the effectiveness of the downstream holes. They also reported an increase in the effectiveness downstream the second row in the double injection compared with the single injection. Using the same technique, Gao et al. [8] measured the cooling effectiveness on both sides of a gas turbine blade and reported an increase in the cooling performance of the laidback fan-shaped holes particularly at high blowing ratios.

The shaped holes are widely used in the modern generation of gas turbine to increase the film cooling capacity downstream the injection point. Immarigeon and Hassan [9] proposed the louver scheme to increase the cooling capacity downstream the injection point by shaping the hole exit. The coolant passes through a bend before being delivered to the exit in order to cool the region upstream the injection point by forced convection. Moreover, this channel increases the film cooling performance downstream the hole by decreasing the jet momentum through the bends in the channel. They investigated numerically, on flat plate, different geometrical parameters to optimize the film cooling performance of the shape exit. They presented a superior performance for the proposed scheme in film cooling performance as well as the conjugate heat transfer contribution. With numerical investigation, Zhang and Hassan [10] showed promising performance for the louver scheme over the curved surface of NASA airfoil. Ghorab et al. [11] using the current facility and the same technique measured experimentally the film cooling performance of the louver scheme over a flat plate.

The previous studies showed promising performance of the louver scheme either numerically or experimentally on a flat plate. However, the performance of the louver over the curved surface of the airfoil has not yet been investigated. The objective of this study is to measure the film cooling performance of the louver scheme over a scaled vane using two-dimensional cascades. Two rows of the louver are distributed at two different locations on the suction side. The performance of the first row is tested while the second row is blocked, and vice versa. Then the coolant is injected through both rows to investigate the performance of the double injection. The low conductivity of the vane material does not allow to measure experimentally the contribution of the louver scheme in increasing the cooling capacity upstream the hole exit.

EXPERIMENTAL SETUP

Test facility and test section

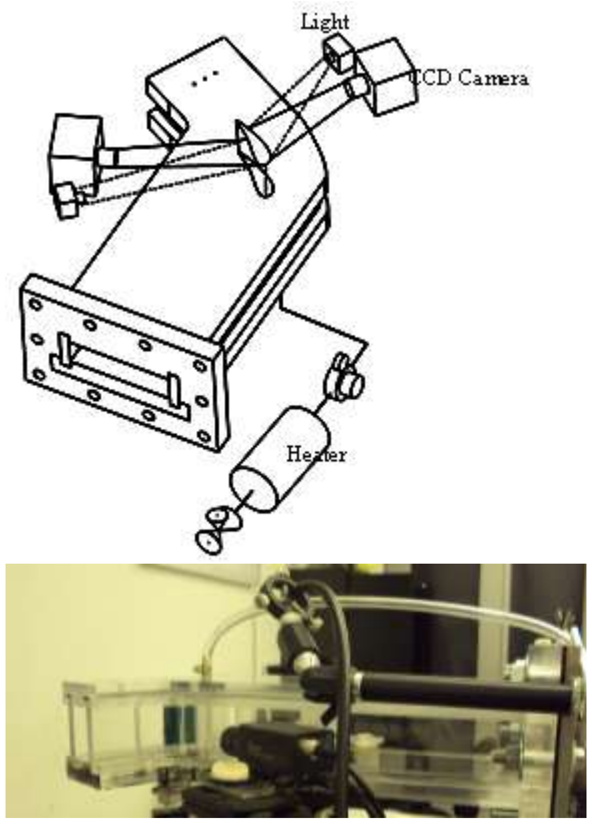

Figure 1. Vane cascade

A subsonic wind tunnel was established at Concordia University to investigate the film cooling performance in gas turbines, the details of the test facility were mentioned by Elnady et al. [12]. The measurements were conducted on a two-dimensional cascade which provides similar flow passages that match similar pressure distribution and curvature of a typical scaled vane used in industrial power generation. The inlet cross section of the cascade is 9.5 cm by 5.1 cm with an additional 30 cm entrance length upstream the vane. All sides of the cascade were machined out of 1.2 cm thick acrylic sheets for optical access. The two side walls were glued to the base while the top plate is designed to be removable in order to ease the handle of the working vanes. Despite manufacturing the test section in acrylic to allow ease of the target area viewing, the side walls are curved walls to simulate the cascade surfaces. These curved surfaces have some corrugations that affect the clarity of the vision. After a few preliminary tests, the camera and the light were positioned slightly facing the transparent side wall and viewed the target area from downstream the vane section. Due to this position, there is no measurement in the area upstream the cooling hole.

The main stream is kept at the room temperature because of the main tank volume limitation, while the secondary flow is heated before being delivered to the test section using a heater with a maximum capacity of 1.2 kW. A small plenum with an internal dimension of 7×2×2cm is assembled at the bottom of the base part of the test section to feed the airfoil with the secondary flow. Fast acting 3-way solenoid valves route the heated jet through a bypass until it achieves steady state conditions. The flow rate in each loop was adjusted manually through gate and needle control valves. A Rosemount Multi-Variable Mass Flow meter (3095MV) is used to measure the main flow, and a rotameter (FL-1502A) is used for the secondary. The main flowmeter records the load pressure and temperature to correct density variations for measuring flow rate. A thermocouple and a pressure sensor are inserted in the plenum to record the static temperature and pressure of the jet before it is delivered to the vane. The density variations on the secondary loop are corrected using the readings of the pressure and the temperature inside the plenum.

The mainstream air is supplied with a volume flow rate of up to 0.5 m^3/s. An additional honeycomb mesh, 5 cm long with a cell size of 0.6 cm, is placed 180 cm upstream the vane leading edge to ensure uniform flow. The trailing edge tailboards were contoured to ensure identical streamline flow downstream the vane. The cascade inlet and exit velocities are set to be 34 m/s and 90 m/s corresponding to Mach numbers 0.1 and 0.23, respectively. The turbulent intensity was measured using PIV technique one chord upstream the vane leading edge and it was found to be 8.5%. The exit Reynolds number based on the axial chord is 200,000 and the vane pressure ratio (P_o/P) is 1.12.

Test vanes and hole configuration

The vanes were made using Stereo lithography (SLA) and a special recess is placed at the middle of the cascade in both the base and top parts to fix the vanes in the cascade. The axial chord C_x is 3.04 cm with a pitch of 5.38 cm to the wall that simulates the adjacent vane. Two rows of holes are distributed on the suction side as shown in Figure 2, and the geometrical details of the louver scheme is shown in Figure 3. The first row is investigated alone, and then the second row and then both rows are investigated together in a stagger arrangement. A different vane is used for each different hole arrangement (first row, second row, both row) and for each hole shape (cylindrical, shaped). Thus a total of 6 vanes are employed with four different blowing ratios (1, 1.35, 1.7, and 2) for each case. The spanwise spacing of the holes located on both rows is 7.5d with 7 holes for the first row, named SS3, and 6 holes for the second row, named SS4. All geometrical details of cooling holes are tabulated in Table 1. A narrow band TLC material in sheet form has been used to map the temperature distribution downstream the film cooling holes. Each vane is manufactured with a groove of 0.254 mm depth downstream the cooling hole. This depth is equal to the TLC sheet thickness in order to allow the mapping of the temperature distribution over the vane surface without disturbing the development of the boundary layer. There is no groove has been manufactured upstream the louver scheme, hence no results has been presented upstream the second row in cases of second row, and double row injections.

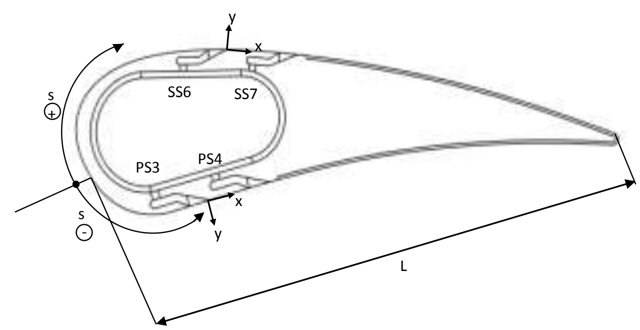

Figure 2. Distribution of the cooling rows around the vane

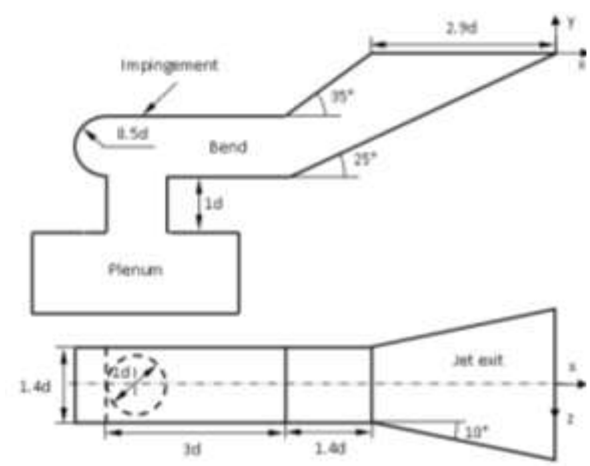

Figure 3. Geometry of louver scheme

Table 1: Cooling hole arrangement

Parameter	SS6	SS7
Location (% of axial chord)	57	67
Hole angle (deg.)	36	24
No. of holes	7	6
Spacing (p/d)	7.5d	

Pressure Measurement and calibration

The pressure distribution around the vane is recorded using a DSA3217/16PX-10psid Scanivalve pressure transducer. The pressure taps on the vane surface are connected to the pressure scanner channels using URTH-063 Urethane flexible tubing with 1.6 mm inside diameter. The differential pressure between the reference point and the measured points is recorded using a software called DSA Link 3.03. Fourteen pressure taps are drilled along the midspan, seven taps on the pressure side, six at the suction side, and a pressure tap on the leading edge just at the stagnant point. A tap located at the suction side of the airfoil close to the leading edge has a mean pressure value between all other tap readings, so it is selected to be the reference point. The readings of all pressure taps are referred to this reference tap reading, and a tap on the pressure scanner is subjected to atmospheric pressure to get the absolute value for each point. During each blow down test, the total pressure and Reynolds number at the test section inlet are maintained in a continuous and steady fashion for intervals of up to 60 seconds. The pressure at each tap is recorded at a rate of 20 Hz and averaged through the running time period. The inlet pressure to the test section is measured one axial chord length upstream of the vane leading edge.

The transient Thermochromatic Liquid Crystal technique (TLC) is used to map the temperature distribution along the vane suction side. New calibration processes has been developed to overcome the difficulties with using the TLC sheets in such curved surface. A special vane is designed for performing the in-situ TLC calibration process without disturbing the boundary layer development on the vane surface. The calibration vane is manufactured similarly to the testing vane but without the film cooling holes. This vane has a special groove of 5cm*5cm*0.36mm in dimensions to contain both the heater and the TLC sheet. The heater (Omega, KH608/205P), with a maximum power output of 0.8W/cm^2, is used to apply a uniform heat flux to the TLC sheet in the calibration process to achieve the same lightening and camera settings for both calibration and experimental running processes. The heater is fed through a DC regulator (BK PRECISION 1623A) to ensure infinitesimal power steps followed by steady state duration.

The calibration vane is placed in the same place as the testing vane and is subjected to the same light and camera conditions as in the experimental. A flexible fiber optic guide is used to get a uniform incident light distribution on the target area. The CCD camera, with 1024×768 pixel resolution, is placed perpendicular to the middle of the target area. A set of RGB images, with different TLC color mappings, is captured at different power inputs while recording the surface temperature at two different positions. The duration between two successive images is long enough to ensure a steady state temperature of the surface, typically 0.25^{o}C difference for two successive steps. This set of images is processed through a developed Matlab code to get the equivalent hue value and relate it to the corresponding recorded temperature. To ensure the precision of the calibration process, the area of interest is meshed through the code into a smaller Region of Interest (ROI). Each ROI is a rectangle of 1 pixel in width with a spatial resolution of 0.1 mm/pixel. In this way, each ROI has its own light intensity and camera angle of view, with similar settings in the experiments.

A uniform rectangular grid of 5 mm spacing is established on the vane surface to account for the curved surface of the vane. The x-distances between grid lines are measured as a number of pixels at different locations along the vane surface and correlated to the actual linear distance.

Data reduction

During the testing, a set of images is captured for 60 seconds at a rate of 5 Hz for a total of 300 images. The region of the upper three holes is selected, to minimize the conduction effect. The color contours in each image are interpreted, using a Matlab code and the calibration data, to temperature contours on the same basis of 1×1 pixel for each Region Of Interest (ROI). The one-dimensional transient heat conduction through a semi-infinite solid is assumed to determine the local heat transfer coefficient and cooling effectiveness. The unsteady heat conduction equation for one dimensional heat conduction into a semi-infinite solid is given as:

$$\rho C_p \frac{\partial T}{\partial t} = \frac{\partial}{\partial y}\left(k \frac{\partial T}{\partial y} \right) \tag{1}$$

with the initial and boundary conditions

$$\left.\begin{aligned} &@ \quad t = 0, \quad T = T_i, \\ &@ \quad y = 0 \quad h\left(T_w - T_f\right) = -k\frac{\partial T}{\partial y} \\ &@ \quad y = \infty \quad T = T_i \end{aligned}\right\} \tag{2}$$

the solution for Equation (1) is given as:

$$\frac{T_w - T_i}{T_f - T_i} = 1 - \exp\left(\frac{h^2 \alpha t}{k^2}\right) erfc\left(\frac{h\sqrt{\alpha t}}{k}\right) \tag{3}$$

The wall temperature, T_w, obtained from the TLC contours, the initial temperature, T_i, of the surface as well as the mainstream temperature, T_m, will be measured by using a thermocouple. The film temperature, T_f, can be calculated as a function of coolant temperature, T_c, mean temperature, and film cooling effectiveness as follows

$$\eta = \frac{\left(T_f - T_m\right)}{\left(T_c - T_m\right)} \tag{4}$$

Equations (3) & (4) are solved together to eliminate the film temperature, T_f, and both equation are then reduced to one equation in two variables, h and η.

$$\begin{aligned} T_w - T_i &= \left[1 - \exp\left(\frac{h^2 \overline{\alpha} t}{k^2}\right) erfc\left(\frac{h\sqrt{\overline{\alpha} t}}{k}\right)\right] \\ &* \left[\eta\left(T_j - T_m\right) + T_m - T_i\right] \end{aligned} \tag{5}$$

where, α and k are the thermal diffusivity and the thermal conductivity of the surface material, respectively. During each running test a set of images is captured for 60 seconds at a rate of 5 Hz for a total of 300 images of 1024*768 pixels. Equation (5) is solved using the least square regression method through the 300 images. Each image represents the wall temperature at a certain time step in the transient experiment, to obtain the local h and η for each ROI.

The calibration vane can be used for measuring the heat transfer coefficient without film cooling over the vane surface. The mainstream flows over the vane by applying a constant heat flux using the electric heater. When achieving a steady state, the CCD camera captures an image of the vane presenting the corresponding temperature contours over the TLC material. The heat transfer coefficient without film cooling can be obtained by applying Equation (6).

$$h_o = q/(T_w - T_m) \qquad (6)$$

The conduction loss from the heater to the vane surface is calculated based on the thermal conductivity and the constant heat flux boundary condition and it is assumed to be 10% from the total heat applied by the heater. The electric loss in the wiring is assumed to be 4% based on the used current, voltage and the wiring cross sectional area. In addition, the radiation loss is assumed to be (1%). The heat losses (q_{loss}) in terms of conduction, electric, and radiation losses are estimated to be fifteen percent of the total heat load applied by the heater (q_{elec}), hence $q = q_{elec} - q_{loss}$, or $q = 0.85\ q_{elec}$

The vane is manufactured using a Stereo lithography technique (SLA) from a material with a commercial brand called WaterShed. The thermal properties of this material are not tabulated on the standard heat transfer tables and were needed to be measured by the authors. Therefore, the measurements of the thermal capacitance, the thermal conductivity, and the thermal diffusivity have been performed and their values found to be, with the given uncertainty, 1.588 ± 0.13548 kJ/kg.K, 0.211328 ± 0.0129 W/m.K, and 0.127E-6 ± 0.1E-7 m^2/s respectively. Uncertainty analysis is based on 95 percent confidence levels, and determined using procedure described by Kline and McClintock [19] and by Moffat [20]. Mach number uncertainty is 0.002, Temperature is ± 0.2^{o}C, pressure is ± 0.2kPa, and the spatial resolution with TLC imaging is 0.1 mm. The uncertainty in determining the exact locations of the thermocouples with respect to local position of each pixel in the calibration process is 0.4^{o}C. These uncertainty leads to ±0.018 in adiabatic effectiveness, about ± 9 percent for a nominal effectiveness of 0.2. The uncertainty in heat transfer coefficient is found to be 33 $W/m^2.K$, about ± 11 percent of averaged span-wise heat transfer coefficient value of 300 $W/m^2.K$

RESULTS AND DISCUSSION

Mach number distribution and heat transfer base line

During each test, the total inlet pressure, one chord upstream the vane leading edge, is maintained constant at 93 kPa. This corresponds to 0.25 exit free stream Mach number and 2E5 exit Reynolds number based on the axial chord. Inlet uniformity is measured at three different pitch-wise locations, one chord upstream of the vane. Static pressure is found to be highly uniform and varies by less than 1 percent of the mean value. The static pressure is measured at fourteen different locations over both sides of the vane. By assuming compressible flow with isentropic flow relations the corresponding Mach number at each location is obtained and plotted in Figure 4 vs. the surface distance of the vane (s) normalized to its actual chord (L). Mach number distribution employed in this study is subsonic on both pressure and suction sides. The pressure expansion yields a corresponding drop in the local temperature along the vane surface. This temperature drop affects the cooling effectiveness as the mainstream temperature changes at different position along the vane midspan. Mach number and temperature distributions of the main stream have been determined from the isentropic gas laws using the pressure readings.

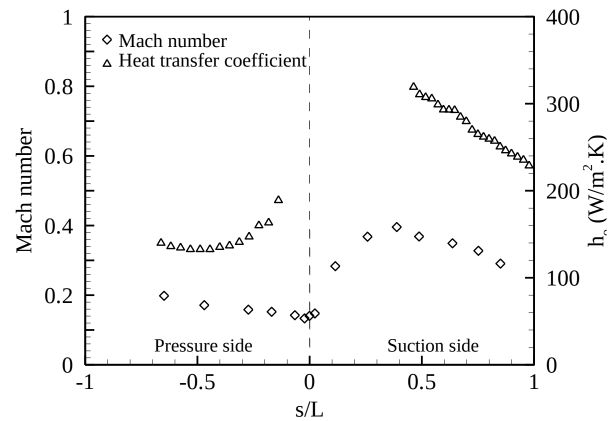

Figure 4. Vane Mach number and baseline heat transfer coefficient distribution

Each airfoil shape has its own streamline that affects the heat transfer over its surface. In addition, the same airfoil itself has different streamline expansions on both the pressure and suction sides. Therefore, the most proper way to present the heat transfer changes on the airfoil surface is by normalizing the heat transfer coefficient of film cooling (h_f) to the heat transfer coefficient without film cooling (h_o). As there is no measurement in the area upstream the cooling holes, the suction side of the vane in this study shows the higher heat transfer coefficient at x/Cx = 0.5, with rapid decay up to the trailing edge. The investigated region is fully turbulent and it is characterized by the adverse pressure gradient and the thickening of the boundary layer.

Cooling effectiveness measurement

The performance of the louver scheme, of base diameter d seen on Figure 3, has been measured at three arrangements; first row alone, second row alone, and both rows together at four blowing ratios 1, 1.35, 1.7, and 2. The performance of the standard cylindrical hole that has the same base diameter and located on the same position, on the vane surface, has been measured at the same blowing ratios. The blowing ratio is calculated based on the flow characteristics of the mainstream at the injection point without film cooling and the jet properties at the base diameter. Figure 5 presents the local distribution of the effectiveness of the louver scheme at the three arrangements and the four blowing ratios compared with the cylindrical hole at the best blowing ratio, Br = 1. The louver scheme single injection provides wider lateral coverage with a longer distance downstream the hole. Increasing the blowing ratio slightly increases the effectiveness just downstream the hole while increasing the lateral coverage mid and far downstream. At Br = 2, the jet lift-off starts to affect the coolant flow and decreases the lateral coverage mid and far downstream. The double injection provides full coverage either for the louver or cylindrical schemes; however the louver provides higher effectiveness all over the protected area.

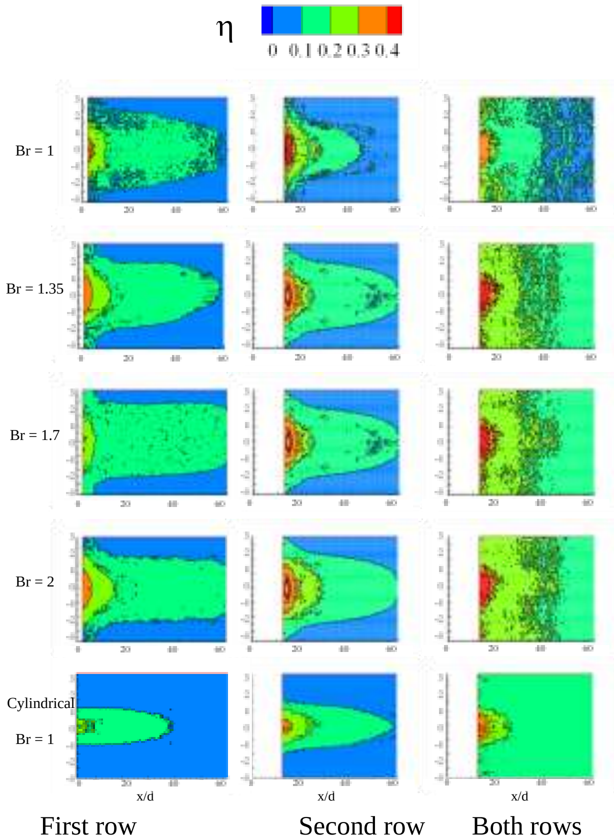

Figure 5. Effectiveness local distribution

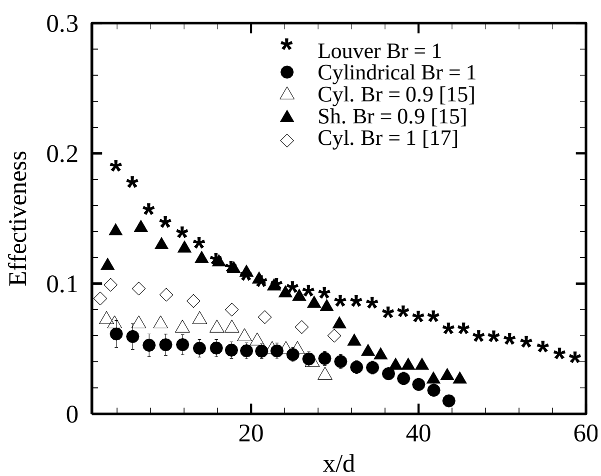

Figure 6. Louver lateral-averaged effectiveness with other geometries

Figure 6 presents the lateral-averaged effectiveness of the louver scheme at Br = 1 vs. the normalized distance downstream the hole exit compared with different geometries. The performances of the cylindrical hole of the present study in addition to cylindrical and shaped hole from previous studies are presented in the same figure. The cylindrical hole shows lower effectiveness compared with the similar hole from Ethridge et al. [17]. This is because the p/d in that study was 5.5 which is equal to two-thirds of the p/d of the current study. The cylindrical hole shows good agreement with the similar hole from Chappell et al. [15]. The performance of the shaped hole on this study is also presented in the figure. The louver scheme shows a higher effectiveness than that of the shaped hole in addition to a longer coverage distance.

Figure 7 presents the lateral-averaged effectiveness of the louver scheme in all cases under investigation compared with the cylindrical hole at the similar locations and blowing

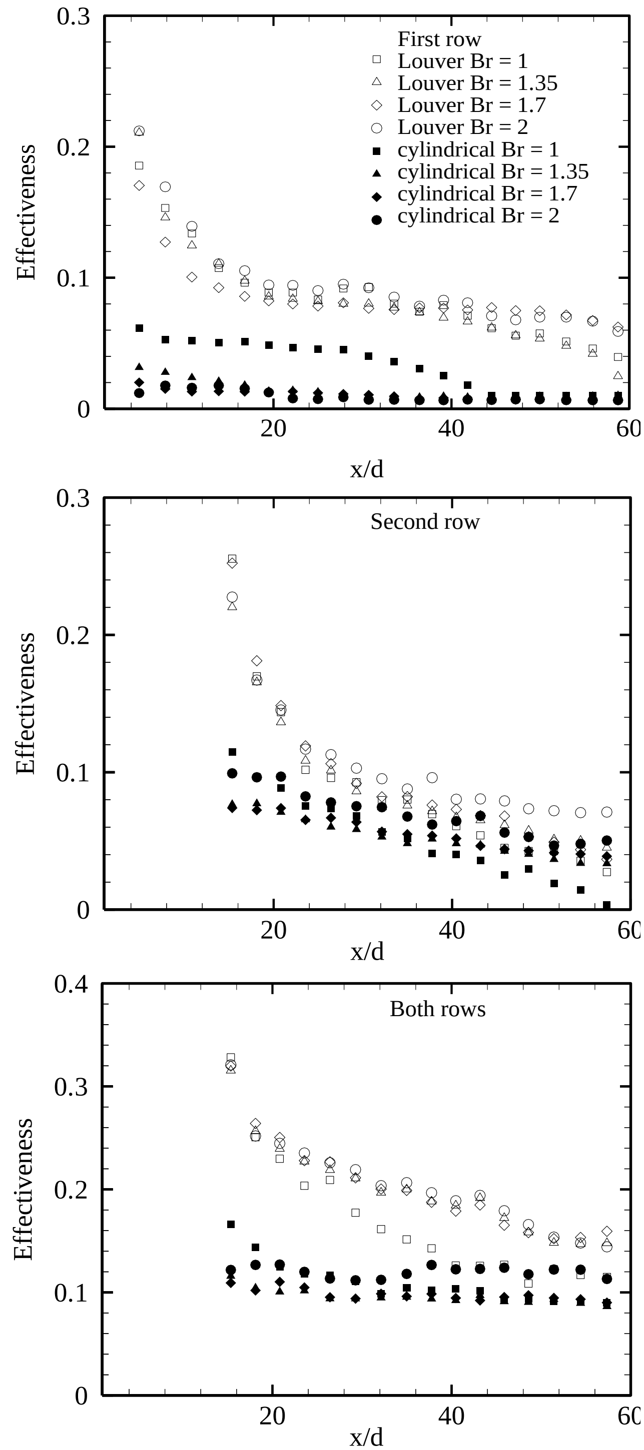

Figure 7. Louver scheme lateral-averaged cooling effectiveness

ratios. The louver exit in general shows better performance than the cylindrical hole for all blowing ratios both in terms of higher effectiveness and longer coverage distance. The louver has superior effectiveness which provides more cooling far downstream than the cylindrical holes near downstream the hole. This indicates the ability of the modified jet to expand laterally early downstream without highly mixing with the mainstream. That is because the well-designed lateral expansion exit allows more jet spreading on the spanwise direction in addition to decreasing the jet momentum. The bends in the louver inlet channel provide a significant decrease in the jet momentum which allows for a larger coolant amount without causing jet lift-off. Therefore, the cooling effectiveness of the louver, on contrary with the standard cylindrical exit, increases with the increase of the blowing ratio due to the significant reduction of the jet momentum.

As the blowing rate increases more coolant is delivered to the jet, causing a higher effectiveness far downstream. The well-mandated jet attaches directly downstream the trailing edge of the hole causing a higher effectiveness. The coolant is then forming an ideal barrier, between the surface and the mainstream, which dilutes gradually with the mainstream. This explains the steep decrease of the effectiveness up to x/d = 20, it then decreases smoothly to the airfoil trailing edge. Changing the position of injection further downstream on the suction side improves the performance of the louver scheme as well as the cylindrical exit as shown in Figure 7. Also, the louver scheme shows superior performance compared with that of the cylindrical holes. For the cylindrical exit, the effectiveness decreases with the blowing ratio giving the maximum effectiveness at Br = 1. This observation means that the jet lift-off starts at this blowing ratio, or lower as lower blowing ratios are not included in this study. The interesting result is that the blowing ratio of 2 keeps a longer effectiveness with relatively higher values compared with other blowing ratio. This indicates that the coolant amount is enough with its momentum to keep an effective barrier between the mainstream and the surface.

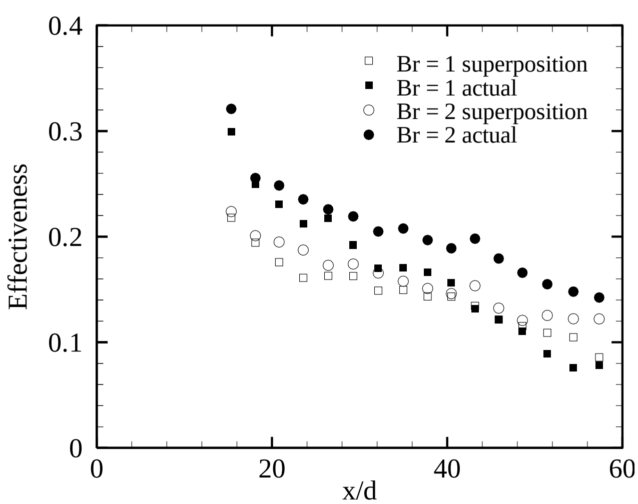

Figure 8. Superposition principle

The interaction between both rows is investigated based on the same coolant amount. The mass of the coolant flowing through the first row is added to that of the second flow and then applied through the plenum to both rows together. The static pressure in the plenum at the case of both rows is higher than that of the first row by 20%. This difference may cause discrepancy in the local blowing ratio at each row yielding a higher coolant amount to flow through the second row. However, this difference cannot be accounted as the objective of this study is to investigate the effect of the interaction between both jets based on the same coolant amount. The results of this investigation are presented in Figure 7 for both exit hole shapes. It must be mentioned that in the case of presenting the three injection cases (first row, second row, both rows) in one figure, the x-coordinates shows the local coordination of each case measured from the trailing edge of the similar cylindrical hole.

The louver scheme with the injection of both rows shows a noticeably better effectiveness than with the second row only due to the coolant accumulation downstream the second row. The first injection location gives longer effectiveness downstream the hole, which allows the remaining coolant to merge with the second injection causing a significant increase in the effectiveness. This shows an additional benefit of the louver scheme, compared with cylindrical exit, as it allows moving the second row further downstream and decreasing the number of rows needed. The principle of superposition is applied to the louver scheme on the suction side. The effectiveness of the first row is added to that of the second row at the points downstream the second row. The summation is plotted in Figure 8 and compared with the real effectiveness of the combined injection. The combined injection shows better performance compared with the superposition, which matches the findings of Zhang and Moon [7].

Heat transfer coefficient

Equation (5) is solved using the least square regression method to obtain both the effectiveness and the heat transfer coefficient. Figure 9 shows the local distribution of the heat transfer coefficient downstream the louver scheme injected from each location and from both locations together. The louver scheme shows a wider heat transfer coefficient distribution just downstream the hole than that of the standard cylindrical hole; however it has slightly lower values. The effect of the coolant from the louver vanished quickly while the cylindrical jet, because of the jet lift-off, disturbs the mainstream up to the trailing edge of the airfoil. The second row injection provides the same heat transfer distribution as the first row, while the double injection yields lower values with wider lateral distribution.

The local heat transfer coefficient at each pixel over the vane surface is divided by the corresponding baseline heat transfer coefficient to be presented in a normalized form. Figure 10 shows the corresponding normalized heat transfer coefficient of the louver scheme for first row at blowing ratios 1 and 2. The effect of the louver on the heat transfer is compared with the similar cylindrical hole from the present study and other cylindrical hole from literature at Br = 1. The cylindrical hole of the present study shows a good agreement with the similar hole from Drost and Bolcs [16]. The louver scheme provides a lower heat transfer coefficient than the cylindrical hole at mid and far downstream the hole, with similar values near downstream. As the blowing ratio increases the jet momentum increases with more disturbance at the interaction region accompanied by stronger vortices causing an increase in the heat transfer coefficient. For all blowing ratios, the mixing between two streams increases with the surface distance increasing, and the coolant completely dilutes in the mainstream causing the heat transfer coefficient to approach unity. The expanded exit allows the jet to spread laterally in addition to the laid-back angle that increases the hydraulic diameter hence decreasing the jet momentum.

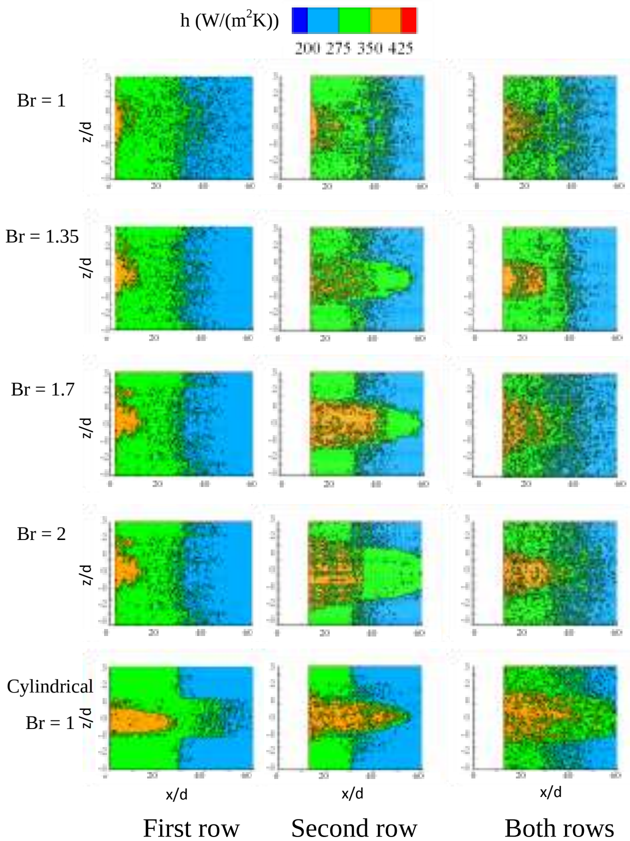

Figure 9. Heat transfer coefficient local distribution

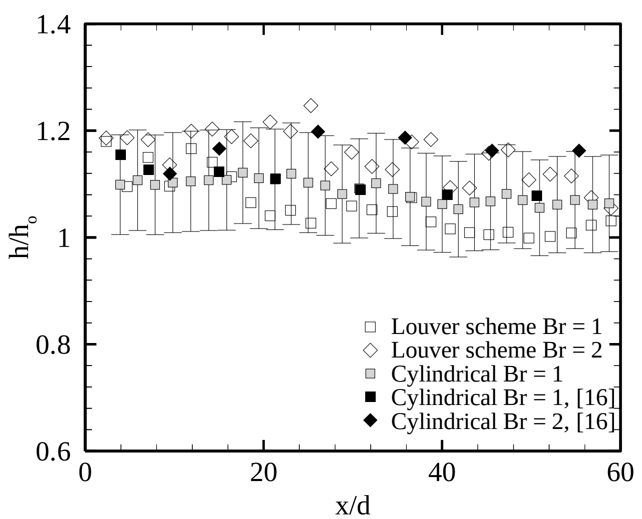

Figure 10. Average-spanwise normalized heat transfer coefficient for the 1st row

Figure 11 presents the effect of the blowing ratio on the heat transfer coefficient for the louver scheme located at the second location and the combined injection. In the standard cylindrical injection, the jet enters the turbulent boundary layer causing a local disturbance and hence increases the heat transfer coefficient. However, the fluctuated flow on the interface between the main stream and the jet causes a rapid diffusion through each other, yielding a mixing between both streams and a decrease in the heat transfer. The higher blowing ratio has the highest h/h_o, however, the difference between all blowing ratios effects is quite well within the measurement uncertainty. The louver scheme presents better heat transfer enhancement due to the expanded exit and it also provided a longer surface distance with better heat transfer. The louver shows, similar to the cylindrical exit, highest h/h_o values at the higher blowing ratios with tendency to unity far downstream.

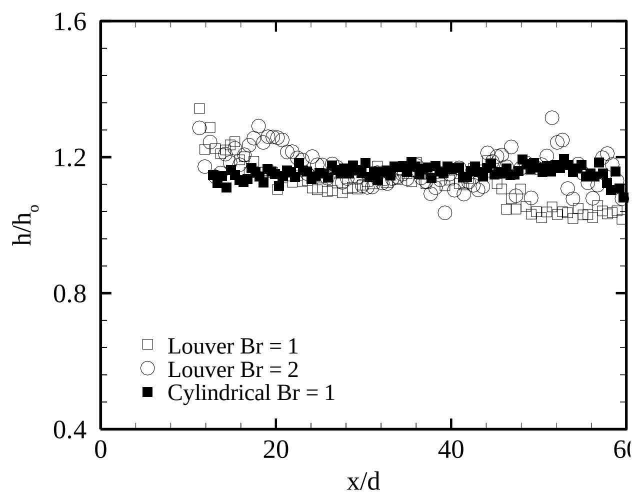

Figure 11. Average-spanwise normalized heat transfer coefficient for the 2nd row

CONCLUSION

The cooling performance of louver scheme has been investigated experimentally for two different positions on the suction side, and has been compared with the standard cylindrical hole of the same base diameter at different blowing ratios. The louver scheme shows superior performance compared with the cylindrical hole in terms of a higher effectiveness, longer effective length downstream the hole, and a lower heat transfer coefficient. The main points highlighted in this study are:

- The louver hole shows a better effectiveness, because of more lateral spreading accompanied with less jet momentum, compared with the standard cylindrical exit with the same coolant amount.
- The second row injection shows better performance with faster decay compared with that of the second row location because of the development of the boundary layer thickness.
- The combined injection shows a slight increase in effectiveness, with better heat transfer due to the favorable interaction between both staggered injections.

The authors recommend a flow visualization investigation, via Particle Image Velocimetry (PIV), for the same running conditions to reveal the phenomena associated to the flow interaction, especially in combined injection.

References

[1] Goldstein, R.J., Eckert, E.R.G., and Burggraf, F., 1974, "Effects of Hole Geometry and Density on Three-Dimensional Film Cooling", International Journal of Heat and Mass Transfer, **17**(5), pp. 595–607.

[2] Gritsch, M., Schulz, A., and Witting, S., 1998, "Adiabatic Wall Effectiveness Measurements of Film Cooling Holes with Expanded Exit," ASME Journal of Turbomachinery, **120**(3), pp. 549-556.

[3] Yu, Y., Yen, C.H., Shih, T.I., Chyu, M.K., and Gogineni, S., 2002, "Film Cooling Effectiveness and Heat Transfer Coefficient Distributions Around Diffusion Shaped Holes," ASME Journal of Heat Transfer, **124**(5), pp. 820-827.

[4] Yuen, C.H.N., and Martinez-Botas, R.F., 2005, "Film Cooling Characteristics of Rows of Round Holes at Various Streamwise Angles in a Crossflow: Part II. Heat Transfer Coefficients," International Journal of Heat and Mass Transfer, **48**(23-24), pp. 5017-5035.

[5] Teng, S., Han, J., and Poinsatte, P.E., 2001, "Effect of Film Hole Shape on Turbine-Blade Heat-Transfer Coefficient Distribution," AIAA Journal of Thermophysics and Heat Transfer, **15**(3), pp. 249-256.

[6] Dittmar, J., Schulz, A., and Wittig, S., 2003, "Assessment of Various Film Cooling Configurations Including Shaped and Compound Angle Holes Based on Large Scale Experiments," ASME Journal of Turbomachinery, **125**(1), pp. 57-64.

[7] Zhang, L., and Moon, H., 2007, "Turbine Blade Film Cooling Study: The Effects of Film Hole Location on the Pressure Side," ASME Paper No. GT2007-27546.

[8] Gao, Z., Narzary, D.P., and Han, J.C., 2008 "Film Cooling on a Gas Turbine Blade Pressure Side or Suction Side with Axial Shaped Holes," International Journal of Heat and Mass Transfer, **51**(9-10), pp. 2139-2152.

[9] Immarigeon, A., and Hassan, I., 2006, "An Advanced Impingement/Film Cooling Scheme for Gas Turbines – Numerical Study," International Journal of Numerical Methods for Heat & Fluid Flow, **16**(4), pp. 470-493.

[10] Zhang, X.Z., and Hassan, I., 2009, "Computational Study of the Effects of Shock Waves on Film Cooling Effectiveness," ASME Journal of Engineering for Gas Turbines and Power, **131**(3), p. 031901.

[11] Ghorab, M.G., Hassan, I., and Lucas, T., 2010, "An Experimental Investigation of Film Cooling Performance of Louver Scheme," ASME Paper No IHTC14- 23262.

[12] Elnady, T., Saleh, W., Hassan, I., Kadem, L., and Lucas, T., 2010, "Experimental Investigation of Louver Cooling Scheme on Gas Turbine Vane Pressure Side," ASME Paper No. IHTC14-22398.

[13] Kline, S. J., and McClintock, F. A., 1953, "Describing Uncertainties in Single-Sample Experiments," ASME Mechanical Engineering, **75**, pp. 3-8.

[14] Moffat, R. J., 1988, "Describing the Uncertainties in Experimental Results"; Experimental Thermal and Fluid Science, **1**(1), pp. 3-17Bogard 2001

[15] Chappell, J., Ligrani, P., Sreekanth, S., and Lucas, T., 2008, "Suction Side Gill Region Film Cooling: Effects of Hole Shape and Orientation on Adiabatic Effectiveness and Heat Transfer Coefficient," ASME Paper No. GT-2008-50798.

[16] Drost, U., and Bolcs, A., 1999, "Investigation of Detailed Film Cooling Effectiveness and Heat Transfer Distributions on a Gas Turbine Airfoil," ASME Journal of Turbomachinery, **121**(2), pp. 233-242.

[17] Ethridge, M.I., Cutbirth, J.M., and Bogard, D.G., 2001, "Scaling of Performance for Varying Density Ratio Coolants on an Airfoil with Strong Curvature and Pressure Gradient Effect," ASME Journal of Turbomachinery, **123**(2), pp. 231-237.